Journal of Sound and Vibration 570 (2024) 118130

Contents lists available at ScienceDirect

Journal of Sound and Vibration

journal homepage: www.elsevier.com/locate/jsvi

Imperfection-induced internal resonance in nanotube resonators

P. Belardinelli [a,*], S. Lenci [a], F. Alijani [b]

[a] Department of Construction, Civil Engineering and Architecture, Polytechnic University of Marche, Ancona, Italy
[b] Department of Precision and Microsystems Engineering, Delft University of Technology, Delft, The Netherlands

ARTICLE INFO

Keywords:
Internal resonance
Carbon nanotube
Molecular dynamics
Imperfect boundary conditions
Thermoelasticity

ABSTRACT

Through molecular dynamics simulations, we demonstrate the possibility of internal resonances in single-walled carbon nanotubes. The resonant condition is engineered with a lack of symmetry in the boundary condition and activated by increasing the energy exchange with a coupled thermal bath. The critical temperature threshold for initiating modal interaction is found to be chirality-dependent. By applying the proper orthogonal decomposition algorithm to molecular dynamics time responses, we show how the thermal fluctuations influence the vibrational behaviour of the nanotube leading to both flexural–flexural and flexural–longitudinal resonances. Understanding the interaction between nanotube resonators and the thermal bath is crucial for designing and optimizing their performance for various nanoscale sensing, actuation, and signal processing applications.

1. Introduction

Modern technologies hinge on tiny vibrating structures [1]. Concealed within every product that enables our creation, communication, sensation, and healing, micro- and nanomechanical systems play a ubiquitous role in various transduction and sensing devices. Beside impacting market products fulfilling breadth of applications [2], fundamental research strongly pursues nanoscale systems [3,4]. Ultra miniaturized systems deploy exceptional capabilities, e.g. highly sensitive sensors provide great resolution at the atomic scale, weigh cells and gas molecules [5,6], measure force between single biomolecules and perform single-protein mass spectrometry [7–9].

Among ultraminiaturized resonators, carbon nanotube (CNT) have demonstrated their superiority [10,11]. A carbon nanotube is a remarkable structure made up solely of carbon atoms. It can be thought of as a graphene sheet rolled up into a cylinder [12]. Outstanding accomplishments originate from a small mass and a high coherence, i.e. very large quality factors offering new opportunities for ultra-sensitive detection schemes [13,14].

Nonetheless, the engineering of these sophisticated devices is far from being straightforward. As the geometric dimensions decrease, it becomes essential to consider the granular nature of matter, and nonlinearities become a crucial factor in the design. Complex phenomena in carbon nanostructures arise from the intricate interplay between binding energy and lattice dynamics. The dynamic characteristics of the phonon spectrum, or phonon modes, offer crucial insights into atomic interactions within the material. Thermal fluctuations influence mechanics unless resonators are adequately cooled to achieve significantly low temperatures. The thermal environment leads to anomalous heat conduction processes within anharmonic systems of such small dimension [15]. However, comprehending the impact of thermal lattice dynamics on stiffness and damping in individual nanoscale systems has proven elusive thus far, primarily due to the experimental complexities associated with manipulating and measuring objects of such diminutive size. Considerable endeavor has been dedicated to analytically and numerically elucidate the mechanics of carbon

* Correspondence to: Department of Construction, Civil Engineering and Architecture (DICEA), Polytechnic University of Marche, Ancona, Italy.
E-mail address: p.belardinelli@univpm.it (P. Belardinelli).

https://doi.org/10.1016/j.jsv.2023.118130
Received 6 September 2023; Received in revised form 16 October 2023; Accepted 24 October 2023
Available online 26 October 2023

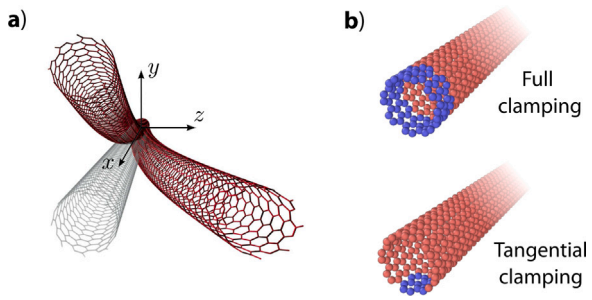

Fig. 1. The nanotube resonator. (a) Constrained-free CNT with a cartesian reference system attached to its constrained edge. The CNTs have length of 20 nm. (b) Boundary conditions: full clamping restraining all the atoms for a length of 0.5 nm (top); tangential clamping (bottom).

nanotubes, including approaches via molecular mechanics [16,17], energy approach [18], tight-binding formalism [19], generalized local quasicontinuum method [20]. Molecular dynamics (MD) simulations play a decisive role, since they provide a platform to investigate the mutual relation between thermal and mechanical properties in carbon nanotubes [21]. By simulating temperature changes and mechanical deformations, it is possible to study how the lattice vibrations (phonons) affect the thermal conductivity of a nanotube, which in turn influences its mechanical response under thermal stress [22]. MD investigations have exposed a pronounced temperature-related variation in the elastic threshold of single-walled carbon nanotubes across a wide spectrum of diameters [23], anisotropic and temperature-dependent properties [24] as well as lattice relaxation and bonds flip [25]. Furthermore, nonlinear effects resulting from lattice dynamics are able to trigger an unprecedented quantity of resonant responses [22] that extend to the macroscopic nonlinear structural vibrating phenomena. The onset of nonlinear regime, i.e. the nonlinear critical amplitude [26], drops dramatically with dimensions while the thermomechanical noise increases. The useful linear dynamic range of nano resonators is severely limited, which means the need to operate in the nonlinear regime [27].

One notable aspect under scrutiny is the distinctive capability of nonlinearities in enabling the transfer of energy between different vibrational modes, even when their resonant frequencies exhibit considerable separation [28–32]. Resonant modal interactions have been a subject of research within the domain of micro and nano resonators [33], with observed phenomena of coherent energy transfer [34] and energy-dependent paths of dissipation [35]. Interaction between mechanical modes brings enhancement in the thermal responsivity of micro-electromechanical resonators [36] and it founds application in RF MEMS filters [37]. Beside the presence of coupled vibrational modes in microbeam resonators, e.g. 1:3 internal resonance was reported in Ref. [38,39], internal resonances have been also investigated in single-walled carbon nanotubes connecting a radial breathing mode (RBM) with a circumferential flexural mode (CFM). This phenomenon is similar to the resonance observed in continuous shells [40].

In this work MD is employed to investigate the interaction between mechanical modes and the thermal environment in the presence of imperfect boundary conditions. The imperfection is introduced to demonstrate how well-engineered small geometrical variations can lead to significant resonant interactions between the nanotube modes of vibration. The Proper Orthogonal Decomposition (POD) algorithm is employed to obtain the orthogonal modes of the vibrations of the single-walled nanotube while accounting for different thermal conditions. For the first time, it is shown a resonant coupling between the longitudinal and flexural modes as well as between higher flexural vibrations in carbon nanotube resonators. The resonant states are demonstrated to be triggered by adjusting the thermal environment. Our POD-based analysis highlights the occurrence of internal resonant behaviours that are responsible for anomalies in the thermoelastic response. This investigation is challenging for inherent complexities such as size-dependence and the interactions with thermal environments [41,42]. Predicting and harnessing resonant interactions becomes especially significant when pursuing applications with ultralow noise requirements (see [26]) and multimode sensing (as discussed in [43]), where modal interactions offer advantages for the nano-mechanical system.

2. Molecular dynamics method and simulation results

Here, our goal is to investigate how Brownian motion varies with temperature in a monolayer carbon nanotube resonator. The device is shown in Fig. 1(a). The dynamics is simulated in the Large-scale Atomic/Molecular Massively Parallel Simulator (LAMMPS) software [44]. To account for atom–atom interactions, we use the Tersoff potential [45] with optimized parameters for lattice dynamics and phonon thermal transport [46]. This potential is commonly used for simulating atomic interactions and predicting mechanical properties of carbon-based nanomaterials [23,47]. In order to monitor the Brownian motion of the nanotube, the atomic model undergoes an initial relaxation process to establish equilibrium at a state of minimal potential. The Polak–Ribiere conjugate gradient algorithm [48] is employed to minimize the total potential energy.

Starting with the initial arrangement of atoms, the minimization process seeks to achieve a local energy minimum, defined as an energy below 1×10^{-10} eV or forces below 1×10^{-10} eV/Å. Following relaxation, constraints are applied to the translational degrees of freedom at one end, determined by the specific clamping configuration. Two different sets of boundary conditions are considered as showcased in Fig. 1(b): (i) The nanotube is free at one end and fully perfectly clamped on the other. This condition restrain all the lattice degrees of freedom for a length of 0.5 nm; (ii) the nanotube is free at one end and tangentially clamped on the other for

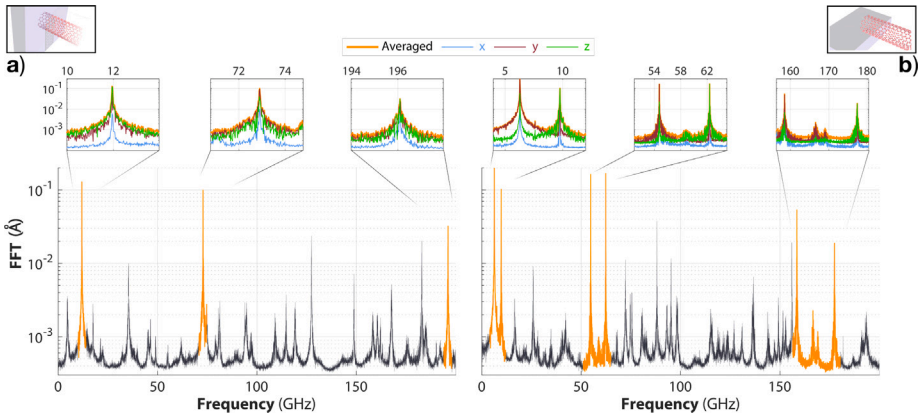

Fig. 2. Frequency spectrum at $T = 50$ K. (a) Averaged FFT of the time response of all atoms for the fully-clamped-free configuration. The first 3 flexural eigenmodes are highlighted. The x, y, z components of the spectrum are detailed in the insets with blue, dark red and green lines, respectively. (b) Averaged FFT for the tangential clamping. The degenerate flexural modes are zoomed in the insets. (For interpretation of the references to color in this figure legend, the reader is referred to the web version of this article.)

0.5 nm. In this case, the degrees of freedom are restricted only for the few atoms close to the support, i.e. at a distance from the lying surface less than 1 Å. The constraint mimics the CNT lying upon a structure such an electrode [13].

Once the equilibrium position is reached, the variations in atomic position and velocity are determined by integrating Newton's equations using the velocity-Verlet algorithm. The integration employs a time step of 0.1 fs. To incorporate thermal effects, the system is equilibrated within a constant volume and temperature ensemble. The temperature is initially adjusted to a specific value and then maintained at a constant level through the application of the Nose–Hoover algorithm, which acts as a thermostat for the translational velocities of the atoms [49]. This thermalization process is applied over a duration of 10 ns to ensure the attainment of a stable temperature. Upon reaching thermal equilibrium, the analysis of vibration response takes place within an energy-conserving ensemble. In this context, the thermal fluctuations of the CNT are observed over a 50 ns period, with an initial transient response of 10 ns being discarded. The coordinates of all atoms are saved at intervals of 2.5 ps.

To determine the resonance frequencies of the CNT, we perform Fast Fourier Transform (FFT) analysis on the extracted time signals obtained from molecular dynamics simulations. An illustrative example of the FFT, averaged over all atoms, is displayed in Fig. 2 for a (8, 8) CNT at 50 K. The chiral index pair, (n, m), defines the structural and electronic properties of a single-walled carbon nanotube [50]. In the fully-clamped configuration the inherent symmetry of the system results in a perfect degeneracy of the flexural modes. As depicted in Fig. 2(a), each flexural mode corresponds to a single peak. It is important to note that every flexural eigenfrequency is connected to two identical eigenmodes oriented in orthogonal directions. Conversely, in the tangential clamping condition (Fig. 2(b)) the axisymmetry is not preserved and each flexural mode is split into two separate flexural eigenmodes (with two different associated eigenfrequencies) in orthogonal transversal directions. The modes are identified by employing proper orthogonal decomposition of the time traces from MD (Appendix A provides a detailed description of this protocol).

3. Effect of temperature

We conduct multiple molecular dynamics simulations involving distinct carbon nanotubes, specifically (5, 10), (8, 8), and (10, 10) configurations. These simulations incorporate a thermal bath covering a temperature range spanning from 5 to 330 K. For each temperature, modal analysis is carried out to monitor the eigenfrequencies. Fig. 3 displays the thermal sensitivity of the third flexural mode of the resonator. Notably, the first and second flexural modes demonstrate the same consistent behaviour, despite the noticeably lower resolution in the thermal shift acquired from molecular dynamics simulations (see Fig. 7 in Appendix A.1). In Fig. 3 we denote by C the complete clamped case and by T the tangentially clamped one. It is illustrated that for temperatures below 200 K there is no discernible impacts between both complete and partial tangential clamping. Indeed, in the tangential configuration, all flexural eigenfrequencies exhibit a thermal dependence comparable to that of the fully clamped tubes across a broad temperature spectrum. This finding underscores the minimal influence of the clamping condition on thermal behaviour. In all the examined geometries the flexural resonance frequencies experience a similar decrease as temperature rises, as depicted in Fig. 3. This phenomenon is described by the Watchman equation [51],

$$E = E_0 - aTe^{-b/T} \tag{1}$$

which is employed to fit the data, and determine the variation of Young's modulus E with temperature from the absolute zero modulus E_0.[1] The temperature independent parameters for data fitting a and b relate to the Grüneisen parameter and the Debye

[1] Naively, the nanotube vibration frequency f is related to the Young's modulus E via $f \propto \sqrt{E}$.

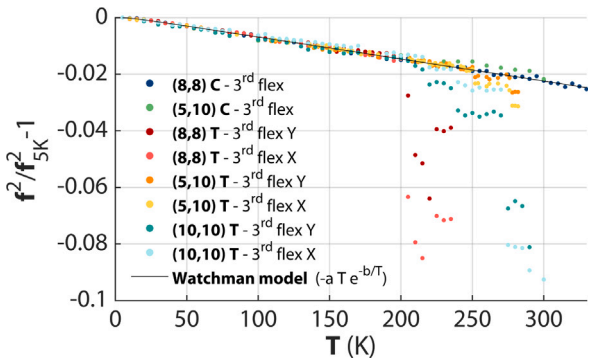

Fig. 3. Eigenfrequencies thermal behaviour. Relative change in frequency with respect to temperature. Estimated coefficients for the Watchman models: $a = 7.805 \times 10^{-5}$, $b = 13.18$.

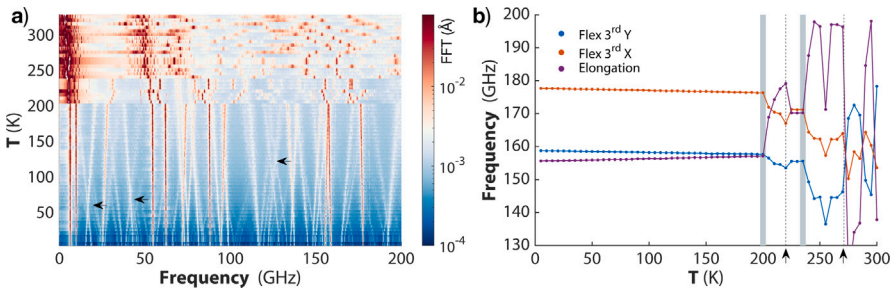

Fig. 4. Internal resonance of higher modes. (a) Density plot of the spectrum showing the thermal shift of the eigenfrequencies. (b) Detailed evolution of the two third flexural and the first longitudinal mode. Region of coinciding eigenfrequencies are highlighted with a grey background. The arrows indicate selected sudden variation of the flexural modes. (For interpretation of the references to color in this figure legend, the reader is referred to the web version of this article.)

temperature, respectively [52]. The rationale behind Eq. (1) lies in the softening of Young's modulus that arises from bond expansion [53]. Considering only the effect of the bond energy weakening due to vibration we have

$$\frac{E(T)}{E_0} \cong 1 - \frac{\int_0^T C_v(t)dt}{\mathrm{E_B}(0)}, \tag{2}$$

in which C_v is the Debye specific heat and $\mathrm{E_B}(0)$ the atomic bond energy at 0 K. The functional dependence of the elastic modulus is detailed in Appendix B.

This consistent behaviour persists until a certain thermostat temperature is reached (200 K for the (8, 8) configuration), beyond which a notable alteration in the mechanical response becomes apparent for the tangentially-clamped device. This effect manifests as a deviation from the observed trend in the eigenfrequency-temperature relation, and indicative of a distinct nonlinear regime coming into play. The anomalies materialize at distinct temperatures for various nanotubes, with the specific temperature points and interactions being contingent on the tube's chirality. Such insight is worth since it links to local material parameters responsible for anomalies in the stiffness and damping [42]. In what follow, we delve into the thermally-induced nonlinear mechanisms.

4. Internal resonant behaviour

In order to understand the root cause of the significant deviation from the Watchman estimation of Fig. 3, we conduct an analysis encompassing the complete spectrum of modes contributing to the motion of the structure. We show in Fig. 4(a) the entire set of eigenfrequencies evolving while varying the bath temperature for the (8, 8) geometry in the tangential clamping configuration. The density plot shows lines with both positive and negative slopes indicating the potential presence of intersections. Occurrence of modal crossing for low-energy modes, i.e. local modes with very low amplitudes, does not bring to significant changes in the global mechanics of the device. Arrows in Fig. 4(a) point to intersections at 60, 70 and 120 K that do not lead to variations in the main modes of the tube (dark red lines).

Interestingly, at 200 K we observe a massive shift in the entire spectrum line. Upon closer examination of the peak trends, it becomes evident that a significant intersection transpires in the vicinity of 155 GHz, which is magnified in Fig. 4(b). The intersection involves the third Y flexural mode and the first longitudinal mode, whose frequencies coincide at the exact temperature of 200 K. A second occurrence for the resonance between the third flexural and the longitudinal modes is also observed at 230 K. The

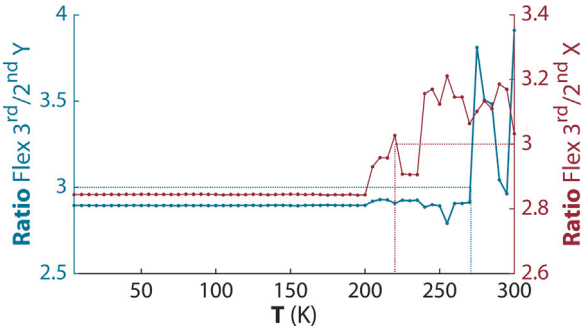

Fig. 5. 3:1 Internal resonance. The thermally-induced resonance between the third and second flexural modes both in Y (left) and X direction (right).

Table 1
Stiffness Ratio ($k_i^{\text{bending}}/k_1^{\text{axial}}$). The ratio is normalized over the geometrical ratio $\frac{I}{AL^2}$.

i	1	2	3
Tangential	7.04×10^{-4}	0.0285	0.3527
Clamped	9.19×10^{-4}	0.0402	0.3663

deviation from the trend depicted in Fig. 3, thus can be attributed to interactions between higher modes of vibrations induced by the system's asymmetry. This special condition at which the ratio of the resonance frequencies of the coupled modes is a rational number is a system internal resonance [54]. This 1:1 internal resonance brings to a sharp downshift for all the flexural modes whereas sudden increase the eigenfrequencies of the longitudinal modes. It manifests as a direct consequence of the opposite thermal behaviour upon flexural and elongating modes of vibration. While flexural eigenmodes soften consequently the bond relaxation, longitudinal modes stiffness with temperature [55]. The phenomenon of thermal behaviour in solids has been comprehensively explained through Grüneisen theory. The expansion or contraction of a solid upon heating hinges on the equilibrium between phonon modes characterized by positive and negative Grüneisen parameters. Transverse acoustic modes, which entail atomic vibrations out of the crystal lattice plane, might manifest negative Grüneisen parameters leading to a negative coefficient of thermal expansion in the axial direction for single-walled carbon nanotubes (-0.9×10^{-6} K^{-1} [56]).

Furthermore, our POD reveals the presence of a radial mode, also referred to as breathing, with thermal stiffening behaviour similar to that of the axial mode (see Fig. 8). In the present study we do not report significant influence of this mode into the dynamics of the tube. However, when activated with an initial phonon velocity sufficiently large, could have an impact bringing 2:1 internal resonances with circumferential flexural modes [40].

Fig. 4(b) presents additional anomalies, indicated by black arrows. These frequency shifts are not associated with longitudinal–transversal resonances, but with transversal–transversal resonances. At 220 and 270 K the third and second flexural modes are in a 3:1 ratio as presented in Fig. 5.

To provide a connection to the mechanics, we analyse the eigenmode shapes computed via the POD. We look at the impact of the boundary condition to the nanotube stiffness. Fig. 6 shows the mode shapes of the first three flexural modes in the tangential clamping configuration. The eigenmodes do not alter with temperature as shown in panels (a)–(c). However, the tangential clamping eigenmodes differs from the usual cantilever shapes and recurring in the fully clamped configuration, as it is showcased in Fig. 6(d)–(f). The calculated eigenmodes are valuable for quantifying the influence of tangential clamping on the mechanical response. To assess this impact, we determine the change in relative stiffness due to imperfect clamping. The equivalent stiffness for flexural and axial eigenmodes are given by [57],

$$k_i^{\text{bending}} = \frac{EI}{L^3} \int_0^1 \left[\Phi_i''(x)\right]^2 dx \tag{3}$$

and

$$k_i^{\text{axial}} = \frac{EA}{L} \int_0^1 \left[\Psi_i'(x)\right]^2 dx, \tag{4}$$

respectively. In Eqs. (4) and (3), the functions $\Phi_i(x)$ and $\Psi_i(x)$ denote the ith flexural and longitudinal eigenmode of the nanotube computed via the POD, E is the Young's modulus, A the cross section area, I is the moment of inertia and L the length of the nanotube. Table 1 summarizes the stiffness ratio between flexural and the first longitudinal modes in the two configurations.

In the context of the tangential clamping scenario, we observe a decrease in the stiffness ratio. This leads to an inherent pathway for energy exchange within the lattice of the unit cell, subsequently enabling the observed internal resonant behaviour.

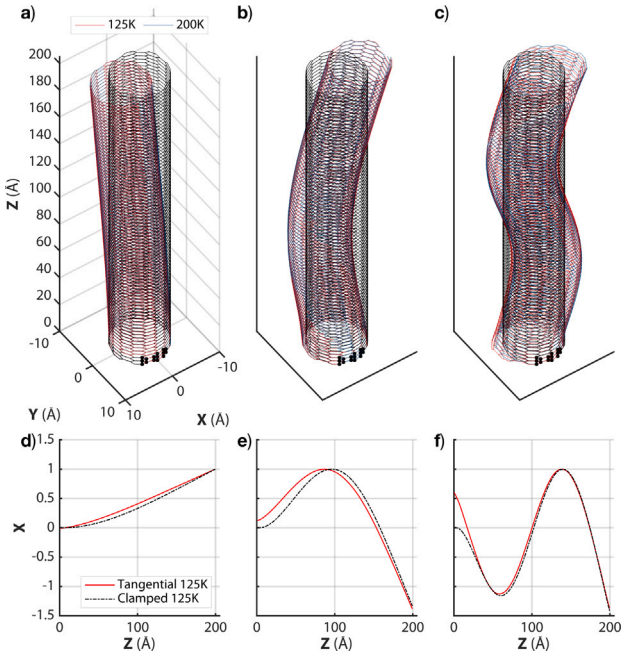

Fig. 6. Eigenmodes and effect of boundary condition. (a)–(c) Mode shapes of the first three flexural modes in the tangential clamping configuration. Eigenmodes at 125 and 200 K are reported in red and black and almost overlap. The undeformed geometry is reported for reference (black lines). (d)–(f) Effect of the boundary condition for the first three flexural modes. The mode shapes are normalized such that $\max \Phi = 1$. (For interpretation of the references to color in this figure legend, the reader is referred to the web version of this article.)

5. Conclusions

Based on molecular dynamics, it is shown that internal resonance in single-walled CNTs can be induced via imperfect boundary conditions. The geometry controls nonlinear coupling between the longitudinal and flexural modes as well as between higher flexural vibrations. The initiation of this internal resonances is controlled by tuning the thermal environment. Although further numerical and experimental verifications are necessary, the idea of thermal activation of modal interaction opens up a promising route towards the engineering of nanotube resonating sensors.

Finally we underline that understanding how local mechanisms by which kinetic energy reallocate among different vibrating modes is a necessity to harness anomalous decay processes and unexpected energy transfers. In this context, the use of classical models are prone to significant errors since thermoelastic parameters become size- and temperature dependent. The enigmatic characterization of nanomechanical resonators still requires an in depth study of the dynamical properties of phonon spectrum and its link to the global dynamics. Essential information of the atomic interactions within the material are the key to unveil particular vibration morphology of the flexural modes and their connection to strong thermal stress effects.

CRediT authorship contribution statement

P. Belardinelli: Proposed the research, Numerical analysis, Prepared the paper. **S. Lenci:** Provided guidance throughout the research, Prepared the paper. **F. Alijani:** Proposed the research, Provided guidance throughout the research, Prepared the paper.

Declaration of competing interest

The authors declare that they have no known competing financial interests or personal relationships that could have appeared to influence the work reported in this paper.

Data availability

Data will be made available on request.

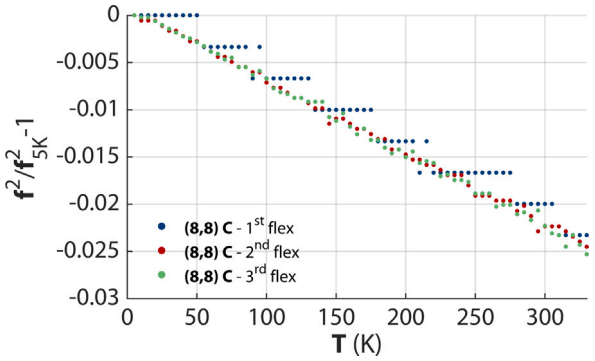

Fig. 7. Relative change of the square of frequency with temperature for the first three flexural modes of the CNT from 5 K to 330 K with a temperature increment of 5 K. The staircase behaviour of the first flexural mode is due to the insufficient resolution in frequency.

Appendix A. Proper orthogonal decomposition

The MD simulations provide the time response in a vector $\mathbf{u}$ comprising the position of $M-$atoms. The time history consists of N snapshots of the motion as $\left[\mathbf{u}(t_1), \mathbf{u}(t_2), \dots, \mathbf{u}(t_N)\right]$. We remove the time average (mean values) of the responses by obtaining the time-varying part, $\mathbf{x}(t_i) = \mathbf{u}(t_i) - \text{mean}(\mathbf{u})$. To extract the proper orthogonal modes of vibrations, a discrete matrix $\mathbf{X}$ is first built such that each row corresponds to a time response of one atom and each column corresponds to a snapshot of the CNT at a specific time as:

$$\mathbf{X} = \begin{bmatrix} \mathbf{x}(t_1) & \mathbf{x}(t_2) & \cdots & \mathbf{x}(t_N) \end{bmatrix} = \begin{bmatrix} x_1(t_1) & \cdots & x_1(t_N) \\ \vdots & \ddots & \vdots \\ x_M(t_1) & \cdots & x_M(t_N) \end{bmatrix}, \tag{5}$$

where $x_i(t_j)$ is the response of the ith atom at time t_j. Once matrix $\mathbf{X}$ is constructed, the orthogonal modes are obtained by using the singular-value decomposition (SVD) of the discrete matrix. The SVD operator decomposes $\mathbf{X}$ as:

$$\mathbf{X} = \mathbf{U}\Sigma\mathbf{V}^*, \tag{6}$$

where $\mathbf{U}$ is an $M \times M$ real or complex unitary matrix, Σ is a $M \times N$ rectangular diagonal matrix with non-negative real diagonals σ_i that are the singular values of $\mathbf{X}$, and $\mathbf{V}$ is an $N \times N$ real or complex unitary matrix, with $\mathbf{V}^*$ being its conjugate transpose. The columns of $\mathbf{U}$ and $\mathbf{V}$ are the so-called left-singular and right-singular vectors of $\mathbf{X}$, respectively. Among these matrices, $\mathbf{U}$ corresponds to proper orthogonal modes of vibration that can linearly obtain all the snapshots of the motion with minimum error. Using this matrix we can identify the modes corresponding to the peaks observed in Fig. 2.

A.1. Frequency resolution

The first three flexural modes highlight the same reduction with respect to the variation of the thermal bath as shown in Fig. 7. The staircase behaviour of the first flexural mode is due to the insufficient resolution in frequency (i.e. 20 MHz).

A.2. Stiffening modes

The thermal stiffening for radial and longitudinal modes is showcased in Fig. 8.

Appendix B. Functional dependence of the elastic modulus

At low temperatures ($T \ll T_D$[2]), Debye's approach results in a specific heat expression [59],

$$C_v = \frac{12\pi^4}{5} N_A k \left(\frac{T}{T_D}\right)^3. \tag{7}$$

By accounting for the electron contribution to specific heat, Eq. (7) modifies in the Einstein–Debye Specific Heat

$$C_v = \frac{\pi^2 N_A k^2}{2E_B(0)} T + \frac{12\pi^4}{5} N_A k \left(\frac{T}{T_D}\right)^3. \tag{8}$$

in which N_A is the Avogadro's number and k the Boltzmann constant. When performing the integral of Eq. (1) it gives a polynomial expression for the Young's modulus variation in the temperature T.

[2] the Debye temperature T_D has been approximately estimated in 2000 K for single-walled CNT [58]

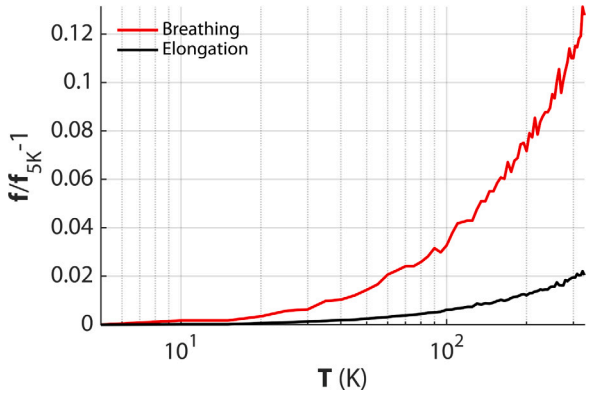

Fig. 8. Relative change of frequency with temperature for the first RBM (breathing) and the longitudinal mode (elongation) for the (8, 8) CNT in the fully clamped configuration. Frequency at 5 K: 34.9 GHz (radial), 127.1 GHz (longitudinal).

References

[1] K.C. Schwab, M.L. Roukes, Putting mechanics into quantum mechanics, Phys. Today 58 (7) (2005) 36–42, http://dx.doi.org/10.1063/1.2012461.

[2] M.A. Huff, MEMS, in: Internet of Things and Data Analytics Handbook, John Wiley & Sons, Ltd, 2017, pp. 147–166, http://dx.doi.org/10.1002/9781119173601.ch9.

[3] M. Li, H.X. Tang, M.L. Roukes, Ultra-sensitive NEMS-based cantilevers for sensing, scanned probe and very high-frequency applications, Nature Nanotechnol. 2 (2) (2007) 114–120, http://dx.doi.org/10.1038/nnano.2006.208.

[4] M. Roukes, Nanoelectromechanical systems face the future, Phys. World 14 (2) (2001) 25.

[5] M. Li, E.B. Myers, H.X. Tang, S.J. Aldridge, H.C. McCaig, J.J. Whiting, R.J. Simonson, N.S. Lewis, M.L. Roukes, Nanoelectromechanical resonator arrays for ultrafast, gas-phase chromatographic chemical analysis, Nano Lett. 10 (10) (2010) 3899–3903, http://dx.doi.org/10.1021/nl101586s.

[6] A.K. Naik, M.S. Hanay, W.K. Hiebert, X.L. Feng, M.L. Roukes, Towards single-molecule nanomechanical mass spectrometry, Nature Nanotechnol. 4 (7) (2009) 445–450, http://dx.doi.org/10.1038/nnano.2009.152.

[7] M.S. Hanay, S. Kelber, A.K. Naik, D. Chi, S. Hentz, E.C. Bullard, E. Colinet, L. Duraffourg, M.L. Roukes, Single-protein nanomechanical mass spectrometry in real time, Nature Nanotechnol. 7 (9) (2012) 602–608, http://dx.doi.org/10.1038/nnano.2012.119.

[8] J. Chaste, A. Eichler, J. Moser, G. Ceballos, R. Rurali, A. Bachtold, A nanomechanical mass sensor with yoctogram resolution, Nature Nanotechnol. 7 (5) (2012) 301–304, http://dx.doi.org/10.1038/nnano.2012.42.

[9] Y.T. Yang, C. Callegari, X.L. Feng, K.L. Ekinci, M.L. Roukes, Zeptogram-scale nanomechanical mass sensing, Nano Lett. 6 (4) (2006) 583–586, http://dx.doi.org/10.1021/nl052134m.

[10] H.-Y. Chiu, P. Hung, H.W.C. Postma, M. Bockrath, Atomic-scale mass sensing using carbon nanotube resonators, Nano Lett. 8 (12) (2008) 4342–4346, http://dx.doi.org/10.1021/nl802181c.

[11] A.K. Hüttel, G.A. Steele, B. Witkamp, M. Poot, L.P. Kouwenhoven, H.S.J. van der Zant, Carbon nanotubes as ultrahigh quality factor mechanical resonators, Nano Lett. 9 (7) (2009) 2547–2552, http://dx.doi.org/10.1021/nl900612h.

[12] M.S. Dresselhaus, G. Dresselhaus, P.C. Eklund, A.M. Rao, Carbon nanotubes, in: The Physics of Fullerene-Based and Fullerene-Related Materials, Springer, 2000, pp. 331–379.

[13] J. Moser, A. Eichler, J. Güttinger, M.I. Dykman, A. Bachtold, Nanotube mechanical resonators with quality factors of up to 5 million, Nature Nanotechnol. 9 (12) (2014) 1007–1011, http://dx.doi.org/10.1038/nnano.2014.234.

[14] K. Jensen, K. Kim, A. Zettl, An atomic-resolution nanomechanical mass sensor, Nature Nanotechnol. 3 (9) (2008) 533–537, http://dx.doi.org/10.1038/nnano.2008.200.

[15] S. Lepri, R. Livi, A. Politi, Thermal conduction in classical low-dimensional lattices, Phys. Rep. 377 (1) (2003) 1–80, http://dx.doi.org/10.1016/S0370-1573(02)00558-6.

[16] T. Chang, H. Gao, Size-dependent elastic properties of a single-walled carbon nanotube via a molecular mechanics model, J. Mech. Phys. Solids 51 (6) (2003) 1059–1074, http://dx.doi.org/10.1016/S0022-5096(03)00006-1.

[17] J.R. Xiao, B.A. Gama, J.W. Gillespie, An analytical molecular structural mechanics model for the mechanical properties of carbon nanotubes, Int. J. Solids Struct. 42 (11) (2005) 3075–3092, http://dx.doi.org/10.1016/j.ijsolstr.2004.10.031.

[18] L. Shen, J. Li, Transversely isotropic elastic properties of single-walled carbon nanotubes, Phys. Rev. B 69 (2004) 045414, http://dx.doi.org/10.1103/PhysRevB.69.045414.

[19] E. Hernández, C. Goze, P. Bernier, A. Rubio, Elastic properties of C and $B_xC_yN_z$ composite nanotubes, Phys. Rev. Lett. 80 (1998) 4502–4505, http://dx.doi.org/10.1103/PhysRevLett.80.4502.

[20] M. Arroyo, T. Belytschko, Nonlinear mechanical response and rippling of thick multiwalled carbon nanotubes, Phys. Rev. Lett. 91 (2003) 215505, http://dx.doi.org/10.1103/PhysRevLett.91.215505.

[21] F. Scarpa, L. Boldrin, H.X. Peng, C.D.L. Remillat, S. Adhikari, Coupled thermomechanics of single-wall carbon nanotubes, Appl. Phys. Lett. 97 (15) (2010) 151903, http://dx.doi.org/10.1063/1.3499748.

[22] B. Sajadi, S. van Hemert, B. Arash, P. Belardinelli, P.G. Steeneken, F. Alijani, Size- and temperature-dependent bending rigidity of graphene using modal analysis, Carbon 139 (2018) 334–341, http://dx.doi.org/10.1016/j.carbon.2018.06.066.

[23] C. Tang, W. Guo, C. Chen, Molecular dynamics simulation of tensile elongation of carbon nanotubes: Temperature and size effects, Phys. Rev. B 79 (2009) 155436, http://dx.doi.org/10.1103/PhysRevB.79.155436.

[24] C.-L. Zhang, H.-S. Shen, Temperature-dependent elastic properties of single-walled carbon nanotubes: Prediction from molecular dynamics simulation, Appl. Phys. Lett. 89 (8) (2006) 081904, http://dx.doi.org/10.1063/1.2336622.

[25] T. Dumitrica, M. Hua, B.I. Yakobson, Symmetry-, time-, and temperature-dependent strength of carbon nanotubes, Proc. Natl. Acad. Sci. 103 (16) (2006) 6105–6109, http://dx.doi.org/10.1073/pnas.0600945103.

[26] M.H. Matheny, L.G. Villanueva, R.B. Karabalin, J.E. Sader, M.L. Roukes, Nonlinear mode-coupling in nanomechanical systems, Nano Lett. 13 (4) (2013) 1622–1626, http://dx.doi.org/10.1021/nl400070e.
[27] H.W.C. Postma, I. Kozinsky, A. Husain, M.L. Roukes, Dynamic range of nanotube- and nanowire-based electromechanical systems, Appl. Phys. Lett. 86 (22) (2005) 223105, http://dx.doi.org/10.1063/1.1929098.
[28] W.J. Venstra, H.J.R. Westra, H.S.J. van der Zant, Q-factor control of a microcantilever by mechanical sideband excitation, Appl. Phys. Lett. 99 (15) (2011) 151904, http://dx.doi.org/10.1063/1.3650714.
[29] T. Faust, J. Rieger, M.J. Seitner, P. Krenn, J.P. Kotthaus, E.M. Weig, Nonadiabatic dynamics of two strongly coupled nanomechanical resonator modes, Phys. Rev. Lett. 109 (2012) 037205, http://dx.doi.org/10.1103/PhysRevLett.109.037205.
[30] K.J. Lulla, R.B. Cousins, A. Venkatesan, M.J. Patton, A.D. Armour, C.J. Mellor, J.R. Owers-Bradley, Nonlinear modal coupling in a high-stress doubly-clamped nanomechanical resonator, New J. Phys. 14 (11) (2012) 113040, http://dx.doi.org/10.1088/1367-2630/14/11/113040.
[31] H.J.R. Westra, D.M. Karabacak, S.H. Brongersma, M. Crego-Calama, H.S.J. van der Zant, W.J. Venstra, Interactions between directly- and parametrically-driven vibration modes in a micromechanical resonator, Phys. Rev. B 84 (2011) 134305, http://dx.doi.org/10.1103/PhysRevB.84.134305.
[32] H.J.R. Westra, M. Poot, H.S.J. van der Zant, W.J. Venstra, Nonlinear modal interactions in clamped–clamped mechanical resonators, Phys. Rev. Lett. 105 (2010) 117205, http://dx.doi.org/10.1103/PhysRevLett.105.117205.
[33] O. Shoshani, S.W. Shaw, Resonant modal interactions in micro/nano-mechanical structures, Nonlinear Dynam. 104 (3) (2021) 1801–1828, http://dx.doi.org/10.1007/s11071-021-06405-3.
[34] C. Chen, D.H. Zanette, D.A. Czaplewski, S. Shaw, D. López, Direct observation of coherent energy transfer in nonlinear micromechanical oscillators, Nature Commun. 8 (1) (2017) 15523, http://dx.doi.org/10.1038/ncomms15523.
[35] J. Güttinger, A. Noury, P. Weber, A.M. Eriksson, C. Lagoin, J. Moser, C. Eichler, A. Wallraff, A. Isacsson, A. Bachtold, Energy-dependent path of dissipation in nanomechanical resonators, Nature Nanotechnol. 12 (7) (2017) 631–636, http://dx.doi.org/10.1038/nnano.2017.86.
[36] Y. Zhang, R. Kondo, B. Qiu, X. Liu, K. Hirakawa, Giant enhancement in the thermal responsivity of microelectromechanical resonators by internal mode coupling, Phys. Rev. A 14 (2020) 014019, http://dx.doi.org/10.1103/PhysRevApplied.14.014019.
[37] A. Vyas, D. Peroulis, A.K. Bajaj, Dynamics of a nonlinear microresonator based on resonantly interacting flexural-torsional modes, Nonlinear Dynam. 54 (1) (2008) 31–52, http://dx.doi.org/10.1007/s11071-007-9326-y.
[38] D.A. Czaplewski, S. Strachan, O. Shoshani, S.W. Shaw, D. López, Bifurcation diagram and dynamic response of a MEMS resonator with a 1:3 internal resonance, Appl. Phys. Lett. 114 (25) (2019) 254104, http://dx.doi.org/10.1063/1.5099459.
[39] S. Houri, D. Hatanaka, M. Asano, R. Ohta, H. Yamaguchi, Limit cycles and bifurcations in a nonlinear MEMS resonator with a 1:3 internal resonance, Appl. Phys. Lett. 114 (10) (2019) 103103, http://dx.doi.org/10.1063/1.5085219.
[40] M.X. Shi, Q.M. Li, Y. Huang, Internal resonance of vibrational modes in single-walled carbon nanotubes, Proc. R. Soc. Lond. Ser. A Math. Phys. Eng. Sci. 465 (2110) (2009) 3069–3082, http://dx.doi.org/10.1098/rspa.2009.0147.
[41] A. Castellanos-Gomez, H.B. Meerwaldt, W.J. Venstra, H.S.J. van der Zant, G.A. Steele, Strong and tunable mode coupling in carbon nanotube resonators, Phys. Rev. B 86 (2012) 041402, http://dx.doi.org/10.1103/PhysRevB.86.041402.
[42] S. Tepsic, G. Gruber, C.B. Møller, C. Magén, P. Belardinelli, E.R. Hernández, F. Alijani, P. Verlot, A. Bachtold, Interrelation of elasticity and thermal bath in nanotube cantilevers, Phys. Rev. Lett. 126 (2021) 175502, http://dx.doi.org/10.1103/PhysRevLett.126.175502.
[43] A. Chandrashekar, P. Belardinelli, S. Lenci, U. Staufer, F. Alijani, Mode coupling in dynamic atomic force microscopy, Phys. Rev. Appl. 15 (2021) 024013, http://dx.doi.org/10.1103/PhysRevApplied.15.024013.
[44] S. Plimpton, P. Crozier, A. Thompson, LAMMPS-large-scale atomic/molecular massively parallel simulator. Sandia national laboratories 18 (2007), 2007.
[45] J. Tersoff, New empirical approach for the structure and energy of covalent systems, Phys. Rev. B 37 (1988) 6991–7000, http://dx.doi.org/10.1103/PhysRevB.37.6991.
[46] L. Lindsay, D.A. Broido, Optimized tersoff and brenner empirical potential parameters for lattice dynamics and phonon thermal transport in carbon nanotubes and graphene, Phys. Rev. B 81 (2010) 205441, http://dx.doi.org/10.1103/PhysRevB.81.205441.
[47] B.I. Yakobson, C.J. Brabec, J. Bernholc, Nanomechanics of carbon tubes: Instabilities beyond linear response, Phys. Rev. Lett. 76 (1996) 2511–2514, http://dx.doi.org/10.1103/PhysRevLett.76.2511.
[48] R. Klessig, E. Polak, Efficient implementations of the Polak–Ribière conjugate gradient algorithm, SIAM J. Control 10 (3) (1972) 524–549, http://dx.doi.org/10.1137/0310040.
[49] D.J. Evans, B.L. Holian, The Nose–Hoover thermostat, J. Chem. Phys. 83 (8) (1985) 4069–4074, http://dx.doi.org/10.1063/1.449071.
[50] L. Qiu, F. Ding, Understanding single-walled carbon nanotube growth for chirality controllable synthesis, Acc. Mater. Res. 2 (9) (2021) 828–841, http://dx.doi.org/10.1021/accountsmr.1c00111.
[51] J.B. Wachtman, W.E. Tefft, D.G. Lam, C.S. Apstein, Exponential temperature dependence of Young's modulus for several oxides, Phys. Rev. 122 (1961) 1754–1759, http://dx.doi.org/10.1103/PhysRev.122.1754.
[52] O.L. Anderson, Derivation of Wachtman's equation for the temperature dependence of elastic moduli of oxide compounds, Phys. Rev. 144 (1966) 553–557, http://dx.doi.org/10.1103/PhysRev.144.553.
[53] M. Gu, Y. Zhou, L. Pan, Z. Sun, S. Wang, C.Q. Sun, Temperature dependence of the elastic and vibronic behavior of Si, Ge, and diamond crystals, J. Appl. Phys. 102 (8) (2007) 083524, http://dx.doi.org/10.1063/1.2798941.
[54] A.H. Nayfeh, D.T. Mook, Nonlinear Oscillations, John Wiley & Sons, 2008.
[55] K. Shirasu, G. Yamamoto, I. Tamaki, T. Ogasawara, Y. Shimamura, Y. Inoue, T. Hashida, Negative axial thermal expansion coefficient of carbon nanotubes: Experimental determination based on measurements of coefficient of thermal expansion for aligned carbon nanotube reinforced epoxy composites, Carbon 95 (2015) 904–909, http://dx.doi.org/10.1016/j.carbon.2015.09.026.
[56] P.K. Schelling, P. Keblinski, Thermal expansion of carbon structures, Phys. Rev. B 68 (2003) 035425, http://dx.doi.org/10.1103/PhysRevB.68.035425.
[57] J. Melcher, S. Hu, A. Raman, Equivalent point-mass models of continuous atomic force microscope probes, Appl. Phys. Lett. 91 (5) (2007) 053101, http://dx.doi.org/10.1063/1.2767173.
[58] R. Waser, Nanoelectronics and Information Technology: Advanced Electronic Materials and Novel Devices, Wiley, 2012.
[59] F.J. Blatt, Modern Physics, McGraw-Hill physics series, McGraw-Hill, 1992.